Digital generation of partially coherent vortex beams

BENJAMIN PEREZ-GARCIA[1,2], ADAD YEPIZ[1], RAUL I. HERNANDEZ-ARANDA[1,*], ANDREW FORBES[2], AND GROVER A. SWARTZLANDER, JR.[3]

[1] Photonics and Mathematical Optics Group, Tecnologico de Monterrey, Monterrey 64849, Mexico
[2] University of the Witwatersrand, Private Bag 3, Johannesburg 2050, South Africa
[3] Rochester Institute of Technology, 54 Lomb Memorial Dr, Rochester, NY, 14623, USA
[*] Corresponding author: raul.aranda@itesm.mx

Compiled June 8, 2016

We present an experimental technique to generate partially coherent vortex beams with arbitrary azimuthal index using only a spatial light modulator. Our approach is based on digitally simulating the intrinsic randomness of broadband light passing through a spiral phase plate. We illustrate the versatility of the technique by generating partially coherent beams with different coherence lengths and orbital angular momentum content, without any moving optical device. Consequently we study its cross correlation function in a wavefront folding interferometer. The comparison with theoretical predictions yields excellent agreement.

OCIS codes: *(030.1640) Coherence; (050.4865) Optical vortices.*

Optical beams that possess helicoidal phase of the form $\exp(il\theta)$ are known as optical vortices (OVs) and carry orbital angular momentum (OAM) of $l\hbar$ per photon [1–3], where the index l is the topological charge. Many interesting applications arise from the study of OVs, for instance optical tweezers and micromanipulation [4–6], optical communications [7, 8] and quantum information [9–12], among others. However, many of these applications are found in the highly spatially coherent regime, leaving aside the partially coherent nature of light.

The theory of coherence has been extensively explored in the past [13, 14]. In our study, we are interested in the transverse spatial coherence which can be described as the capability that two separate points in space at the same z-plane have to interfere. Physically, this can be realized by an extended source where each point in it emits light independently with no fixed phase relationship between each other. The coherence properties of the field produced by this kind of source is mainly studied through the correlation functions of the optical field [15, 16]. In particular, the cross-correlation function (CCF) of a partially coherent vortex beam has been shown to possess a ring dislocation related to the transverse extent of the source [17, 18], in contrast to the characteristic doughnut shape observed in the intensity profile of a highly coherent vortex beam.

There are many ways to experimentally generate partially coherent OVs. For instance, broadband white light passing through a Spiral Phase Plate (SPP) seems the natural way to create them [19]. Another method involves the focusing of laser light onto a rotating ground glass disk which is then redirected onto a spatial light modulator (SLM) displaying a fork-like hologram [20, 21]. Partially coherent Bessel beams have also been generated through Gerchberg and Saxton holograms [22] and by non-interferometric techniques [23]. In all cases, controlling the coherence is not a straightforward task and in some instances this is achieved by moving specific optical elements, i.e. lenses or apertures. In this Letter we propose an all-digital technique to construct partially coherent OVs by using only a SLM, where we can easily select the OAM and spatial coherence quantitatively.

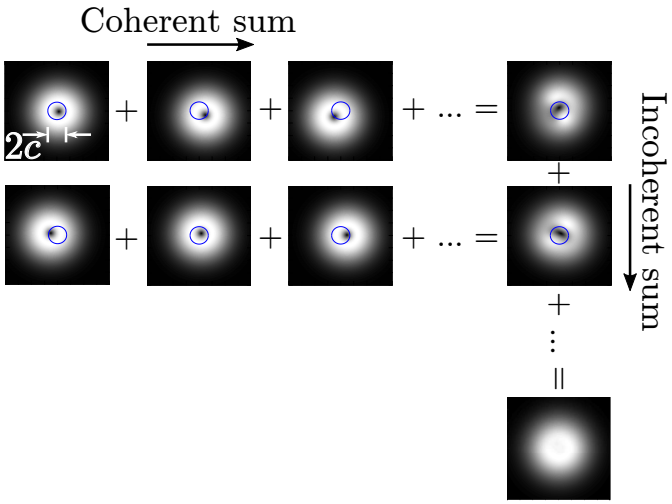

Fig. 1. Schematic representation of partially coherent vortex beams. The blue circles show the boundaries for the vortex superposition to create one member of the ensemble.

We begin our analysis with a homogeneously polarized fully coherent vortex beam at the plane $z = 0$ [3, 24], with its center located at $(x, y) = (0, 0)$, given by

$$u_l(x, y) = (r/w_0)^{|l|} \exp(-r^2/w_0^2) \exp(il\theta), \quad (1)$$

where $r = \sqrt{x^2 + y^2}$ is the radial coordinate, $\theta = \tan^{-1}(y/x)$ is the azimuthal angle, w_0 is the waist of the Gaussian envelope, and l is the topological charge. In order to represent a partially

coherent optical vortex we construct a field at any point on the xy plane as the ensemble average of randomly displaced beams having random phases. Each member of the ensemble has amplitude and phase profiles that are constructed by the coherent superposition of N vortex beams of the form given by Eq. 1, whose centers are uniformly distributed at random locations within a finite circle as shown in Fig. 1. In this way, we can express a member of the ensemble as

$$E_k(x,y) = \sum_{j=0}^{N} u_l(x-a_j, y-b_j)\exp(i\phi_j), \tag{2}$$

where the coordinates (a_j, b_j) are random numbers uniformly distributed within a circle of radius c, and represent the locations of each of the individual randomly located vortices. As can be seen in Eq. 2, each of the individual vortices u_l is also multiplied by a random phase term $\exp(i\phi_j)$, in which ϕ_j is uniformly randomly distributed between 0 and 2π. The field expressed in Eq. 2 represents a member of the ensemble and can be experimentally generated by means of a spatial light modulator, in order to construct the full ensemble a sequence of computer generated holograms of such fields is sent to the SLM, a different CGH for each frame. The partially coherent properties of our simulated source require us to look for correlations of the field at different points on the plane of the detector, this is done through the computation of intensity and cross-correlation functions. These can be expressed as follows

$$I_k(r,\theta) = E_k(r,\theta)E_k^*(r,\theta), \tag{3}$$
$$\chi_k(r,\theta) = \mathrm{Re}\{E_k(r,\theta)E_k^*(r,\theta+\pi)\}, \tag{4}$$

where for convenience we expressed both functions in cylindrical polar coordinates (r,θ) and * stands for the complex conjugate.

The beam distribution at the plane of the detector is described by the ensemble average of random fields, in this case by the incoherent superposition of M realizations of the composite beam given in Eq. 2. These ensemble average intensity and cross-correlation functions at the plane of the detector are achieved by letting the detector do the integration over the total number M of frames in one exposure time, mathematically these ensemble average quantities can be written as [17]

$$\langle I(r,\theta)\rangle = \frac{1}{M}\sum_{k=0}^{M} I_k(r,\theta), \tag{5}$$
$$\langle \chi(r,\theta)\rangle = \frac{1}{M}\sum_{k=0}^{M} \chi_k(r,\theta). \tag{6}$$

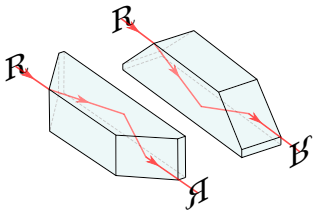

Fig. 2. Schematic representation of the Dove prism. Observe that the Dove prism inverts and rotates the image. Furthermore, notice that the angle between the output of both Dove prisms is 180°.

An experimental realization of the cross-correlation function given by Eq. 4 requires a measurement of the correlation between pairs of points in the field that are diametrically opposed, this can be can be achieved experimentally using a wavefront folding interferometer in which Dove prisms (DP) are used to invert the beams with respect to the horizontal or vertical axis as shown in Fig. 2.

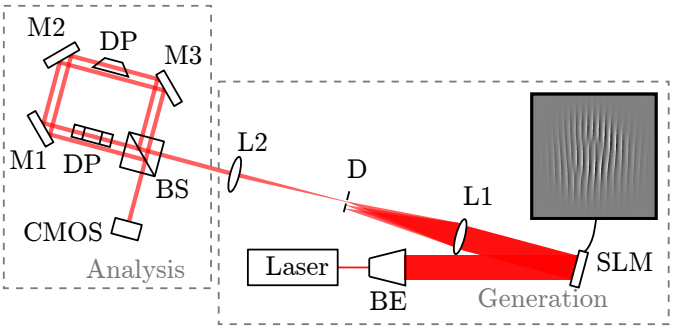

Fig. 3. Experimental setup. HeNe Laser; BE: Beam Expander; L1–L2: lenses; D: iris diaphragm; SLM: Spatial Light Modulator; BS: Beam Splitter; DP: Dove Prism; M1–M3: Mirrors; CMOS: Camera.

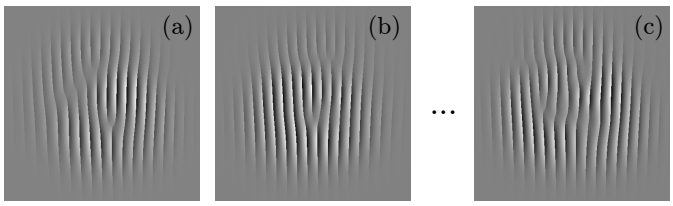

Fig. 4. Examples of holograms displayed in the SLM. (a) Shows the first frame, (b) second frame and (c) last frame, for a partially coherent OV with topological charge $l = 1$.

Figure 3 shows the experimental setup to digitally generate and analyze partially coherent vortex beams. To generate a partially coherent vortex beam, we employed a linearly polarized HeNe laser source ($\lambda = 632.8$ nm) and a beam expander to shine the laser onto a spatial light modulator (HoloEye PLUTO VIS SLM with 1920×1080 pixels of pitch 8 μm and calibrated for a 2π phase shift at $\lambda = 632.8$ nm) displaying a movie at 60 Hz. Each frame of the movie contains a different hologram, each one corresponding to a different member of the ensemble generated according to Eq. 2 through the coherent superposition of $N = 500$ randomly distributed vortex beams (see Fig. 4). It is important to remark that each hologram depicted in Fig. 4 already corresponds to the superposition of the field $E_k(x,y)$ using $N = 500$ terms. In this case, we created a total ensemble of $M = 200$ members, this means that we generated a total of 200 holograms, which are computationally generated in a previous process before sending them to the SLM. A system of two lenses (L1 and L2) are used to select and reconstruct the field in the first diffracted order coming out of the SLM. In order to characterize the field that we constructed we need to look at the ensemble average CCF of Eq. 6 as we previously discussed. Once the partially coherent beam has been generated at the SLM, it is sent as the input to a wavefront folding Sagnac interferometer through a non-polarizing beam splitter (BS) which divides the beam into two equal copies. Each of the two beam copies passes through

a rotated DP with the orientation shown in Fig. 3 and they are eventually recombined at the same beam splitter. Finally, the interference pattern was recorded using a CMOS sensor (Firefly FMVU-13S2C) by adjusting its frame rate to match that of the SLM, and the shutter time parameter in order for the detector to be able to integrate over 200 frames, which amounts to a total exposure time of approximately 3.4s.

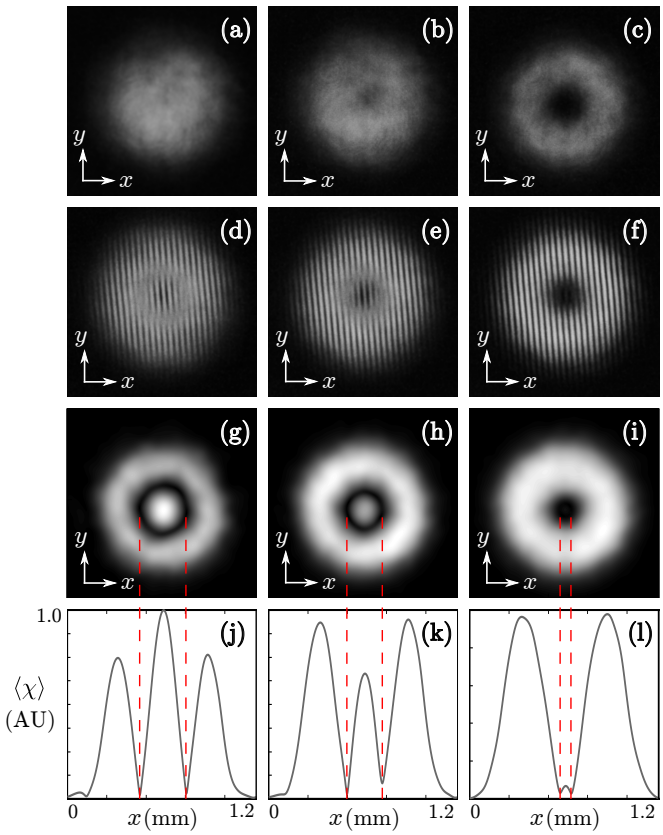

Fig. 5. Experimental results for different coherence lengths. From left to right, the coherence length increases. First row shows the intensity of the beam, second row shows the experimental CCF, third row shows a Fourier filtered version of the experimental CCF, last row shows the CCF profile along the x–axis ($y = 0$).

The existence of the vortex structure in a partially spatially coherent beam is evidenced as a ring dislocation in its CCF [17, 25]. The transverse coherence length can be expressed as [14]

$$L_c = \frac{0.61\lambda}{c} d, \tag{7}$$

where λ is the wavelength, c corresponds to the radius of the circular region where the random superposition of vortices occurs, and d is the distance to the plane of the screen where the field is observed. Furthermore, the ring dislocation radius and the radius of the region where the random vortices are uniformly distributed are related by [17]

$$\frac{R}{w} = \frac{c}{c+w}, \tag{8}$$

where w is the waist of the Gaussian background envelope, R is the radius of the ring dislocation in the CCF, and c is the radius of the circular region.

As stated by Eq. 8, the size of the ring dislocation radius is related to the spatial coherence properties of the beam. Note that if the value of c is increased, the transverse spatial coherence at the plane of the screen decreases, the vortex beam becomes more diffuse, the beam spread widens, and the ring dislocation radius in the CCF also increases. In Figure 5 we show the experimental results for the intensities and corresponding cross-correlation functions for a partially coherent vortex, with $l = 1$, an three different coherence lengths. From left to right the coherence length is increased and we observe that the ring dislocation in the cross-correlation function is smaller as the coherence is increased. It should also be noted that as the coherence of the beam increases the doughnut shape intensity profile, which is characteristic of coherent vortices, starts to become evident. In order to increase (or decrease) the coherence of the beam, we generate holograms where the superposition of the random vortex beams occurs in a circular region of smaller (or bigger) radius, see Fig. 1, in other words we change the value of c. In this sense, we are effectively changing the transverse coherence length of the beam without moving any optical element, i.e. without the use of rotating ground glass plates or focusing lenses.

Table 1. Experimental versus theoretical values of the ring dislocation radius.

c [mm]	R_{Theory} [mm]	R_{Measured} [mm]	Error [%]
0.640	0.300	0.301	0.33
0.400	0.234	0.230	1.71
0.080	0.070	0.071	1.43

In Table 1 we show a comparison between the predicted theoretical values for the ring dislocation radius, calculated according to Eq. 8, versus the experimental results. These values correspond to $l = 1$, with a background beam waist of $w = 0.568$mm, which translate into 71 pixels on the SLM, considering that the pixel size is 8μm. The results show very good agreement between the measured and theoretically predicted values, the percentage error is calculated as $|R_{\text{Theory}} - R_{\text{Measured}}|/R_{\text{Theory}} \times 100$.

It has also been shown in Refs [20, 25, 26] that the number of ring dislocations appearing in the CCF is in a one to one correspondence with the topological charge of a partially coherent OV. This feature of the partially coherent vortex was also validated with our experimental technique, the optical setup shown in Fig. 3 was also used to demonstrate the relationship between the OAM in a digitally generated partially coherent vortex and the number of ring dislocations present in the CCF. Figure 6 shows the cross-correlation functions for different topological charges, $l = 1, 2$, and 3. For the three cases, the intensity profile on the screen is just a bright spot, however their cross-correlation functions exhibit ring dislocations that are in a one-to-one correspondence with the topological charge. In order to change the value of the topological charge we need to generate holograms with a random superposition of individual vortex beams all carrying the desired azimuthal index equal to l.

In conclusion we carried out two experiments to show the generation of spatially partially coherent vortex beams using only an SLM as a digital means for their construction. This technique provides control over the transverse coherence length of a beam, as demonstrated by our first experiment showing the generation of a partially coherence vortex with varying co-

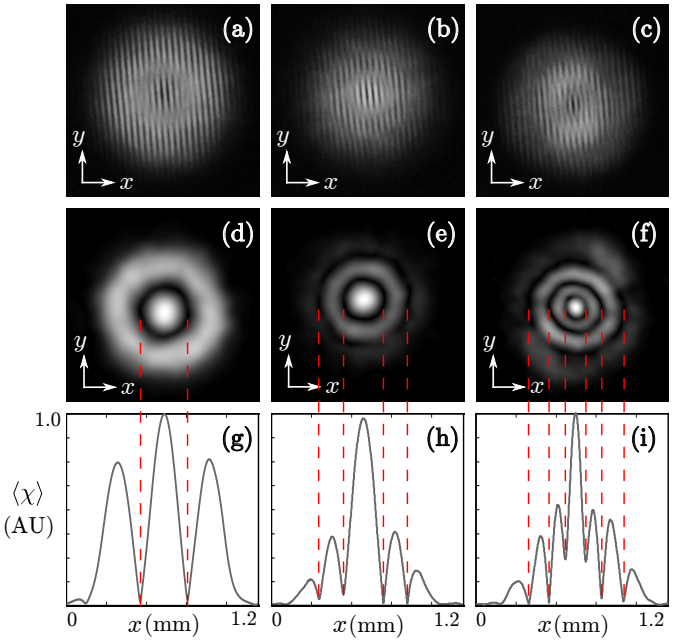

Fig. 6. Cross-correlation function for partially coherent vortex beams with different topological charges: (a) $l = 1$, (b) $l = 2$ and (c) $l = 3$. (d) – (f) show the Fourier filtered version of the experimental CCF in the same order. (g) – (i) show the CCF profile along the x–axis ($y = 0$).

herence lengths for a fixed value of OAM content ($l = 1$). We observed the ring dislocation in the CCF experimentally and demonstrated that its radius is dependent on the spatial coherence of the beam. Moreover, the second experiment validates the relationship between the OAM content and the number of dislocation rings observed in the CCF, which allows a direct determination of the topological charge by counting the number of ring dislocations in the CCF. The proposed method effectively simulates the behavior of a partially coherent OV, it is a versatile technique and it also paves the way for further studies on coherence, such as the study of vector singularities in partially coherent fields as in the work of Chernyshov et al.[27], or in the fields of optical communications and imaging systems where coherence plays a key role.

Funding. Consejo Nacional de Ciencia y Tecnología (grant 158174).

REFERENCES

1. L. Allen, M. W. Beijersbergen, R. J. C. Spreeuw, and J. P. Woerdman, "Orbital angular momentum of light and the transformation of Laguerre-Gaussian laser modes," Phys. Rev. A **45**, 8185–8189 (1992).
2. A. M. Yao and M. J. Padgett, "Orbital angular momentum: origins, behavior and applications," Adv. Opt. Photon. **3**, 161–204 (2011).
3. M. Padgett and R. Aspden, "Orbital Angular Momentum of Light," in "Laser Beam Propagation: Generation and Propagation of Customized Light," , A. Forbes, ed. (CRC Press, 2014).
4. H. He, M. E. J. Friese, N. R. Heckenberg, and H. Rubinsztein-Dunlop, "Direct Observation of Transfer of Angular Momentum to Absorptive Particles from a Laser Beam with a Phase Singularity," Phys. Rev. Lett. **75**, 826–829 (1995).
5. N. B. Simpson, K. Dholakia, L. Allen, and M. J. Padgett, "Mechanical equivalence of spin and orbital angular momentum of light: an optical spanner," Opt. Lett. **22**, 52–54 (1997).
6. C. López-Mariscal, J. C. Gutiérrez-Vega, G. Milne, and K. Dholakia, "Orbital angular momentum transfer in helical Mathieu beams," Opt. Express **14**, 4182–4187 (2006).
7. G. Gibson, J. Courtial, M. J. Padgett, M. V. Vasnetsov, V. Pas'ko, S. M. Barnett, and S. Franke-Arnold, "Free-space information transfer using light beams carrying orbital angular momentum," Opt. Express **12**, 5448–5456 (2004).
8. J. Wang, J.-Y. Yang, I. M. Fazal, N. Ahmed, Y. Yan, H. Huang, Y. Ren, Y. Yue, S. Dolinar, M. Tur *et al.*, "Terabit free-space data transmission employing orbital angular momentum multiplexing," Nature Photonics **6**, 488–496 (2012).
9. G. Molina-Terriza, J. P. Torres, and L. Torner, "Management of the Angular Momentum of Light: Preparation of Photons in Multidimensional Vector States of Angular Momentum," Phys. Rev. Lett. **88**, 013601 (2001).
10. A. C. Dada, J. Leach, G. S. Buller, M. J. Padgett, and E. Andersson, "Experimental high-dimensional two-photon entanglement and violations of generalized Bell inequalities," Nat. Phys. **7**, 677–680 (2011).
11. M. Mafu, A. Dudley, S. Goyal, D. Giovannini, M. McLaren, M. J. Padgett, T. Konrad, F. Petruccione, N. Lütkenhaus, and A. Forbes, "Higher-dimensional orbital-angular-momentum-based quantum key distribution with mutually unbiased bases," Phys. Rev. A **88**, 032305 (2013).
12. B. Perez-Garcia, J. Francis, M. McLaren, R. I. Hernandez-Aranda, A. Forbes, and T. Konrad, "Quantum computation with classical light: The Deutsch Algorithm," Physics Letters A **379**, 1675 – 1680 (2015).
13. M. Born, E. Wolf, A. Bhatia, P. Clemmow, D. Gabor, A. Stokes, A. Taylor, P. Wayman, and W. Wilcock, *Principles of Optics: Electromagnetic Theory of Propagation, Interference and Diffraction of Light* (Cambridge University Press, 2000).
14. A. Marathay, *Elements of optical coherence theory*, Wiley series in pure and applied optics (Wiley, 1982).
15. G. Gbur, "Simulating fields of arbitrary spatial and temporal coherence," Opt. Express **14**, 7567–7578 (2006).
16. F. S. Roux, "Topological charge densities in inhomogeneous stochastic optical fields," Journal of Optics **17**, 045610 (2015).
17. G. A. Swartzlander and R. I. Hernandez-Aranda, "Optical Rankine Vortex and Anomalous Circulation of Light," Phys. Rev. Lett. **99**, 163901 (2007).
18. G. Gbur and J. Grover A. Swartzlander, "Complete transverse representation of a correlation singularity of a partially coherent field," J. Opt. Soc. Am. B **25**, 1422–1429 (2008).
19. D. M. Palacios, I. D. Maleev, A. S. Marathay, and G. A. Swartzlander, "Spatial Correlation Singularity of a Vortex Field," Phys. Rev. Lett. **92**, 143905 (2004).
20. C. Zhao, F. Wang, Y. Dong, Y. Han, and Y. Cai, "Effect of spatial coherence on determining the topological charge of a vortex beam," Applied Physics Letters **101**, 261104 (2012).
21. Y. Chen, F. Wang, C. Zhao, and Y. Cai, "Experimental demonstration of a Laguerre-Gaussian correlated Schell-model vortex beam," Opt. Express **22**, 5826–5838 (2014).
22. C. R. Alves, A. J. Jesus-Silva, and E. J. S. Fonseca, "Self-reconfiguration of a speckle pattern," Opt. Lett. **39**, 6320–6323 (2014).
23. J. A. Rodrigo and T. Alieva, "Rapid quantitative phase imaging for partially coherent light microscopy," Opt. Express **22**, 13472–13483 (2014).
24. L. Allen, M. Padgett, and M. Babiker, "{IV} The Orbital Angular Momentum of Light," (Elsevier, 1999), pp. 291 – 372.
25. Y. Yang, M. Mazilu, and K. Dholakia, "Measuring the orbital angular momentum of partially coherent optical vortices through singularities in their cross-spectral density functions," Opt. Lett. **37**, 4949–4951 (2012).
26. A. Yepiz Escalante, B. Perez-Garcia, R. I. Hernandez-Aranda, and G. A. Swartzlander, "Determination of angular momentum content in partially coherent beams through cross correlation measurements," Proc. SPIE **8843**, 884302–884302–8 (2013).
27. A. A. Chernyshov, C. V. Felde, H. V. Bogatyryova, P. V. Polyanskii, and M. S. Soskin, "Vector singularities of the combined beams assembled from mutually incoherent orthogonally polarized components," Journal of Optics A: Pure and Applied Optics **11**, 094010 (2009).